THE JOURNAL OF BIOLOGICAL CHEMISTRY VOL. 288, NO. 46, pp. 32941–32951, November 15, 2013

Inositol 1,4,5-Trisphosphate (IP_3) Receptor Up-regulation in Hypertension Is Associated with Sensitization of Ca^{2+} Release and Vascular Smooth Muscle Contractility*[S]

Received for publication, June 25, 2013, and in revised form, September 20, 2013 Published, JBC Papers in Press, October 4, 2013, DOI 10.1074/jbc.M113.496802

Haissam Abou-Saleh[‡], Asif R. Pathan[§], Arwa Daalis[‡], Satanay Hubrack[‡], Hamda Abou-Jassoum[¶], Hamda Al-Naeimi[¶], Nancy J. Rusch[§], and Khaled Machaca[‡1]

From the [‡]Department of Physiology and Biophysics, Weill Cornell Medical College in Qatar, Qatar Foundation, Education City, Doha 24144, Qatar, the [§]Department of Pharmacology and Toxicology, University of Arkansas for Medical Sciences, Little Rock, Arkansas 72205, and the [¶]Department of Biological and Environmental Sciences, Qatar University, Doha 2713, Qatar

Background: The role of the vascular IP_3 receptor (IP_3R) in hypertension is unknown.
Results: IP_3R are up-regulated in vascular smooth muscle (VSM) in hypertension through the calcineurin-NFAT pathway.
Conclusion: Up-regulated IP_3R in VSM sensitize Ca^{2+} release and enhance contraction.
Significance: Up-regulated vascular IP_3R may contribute to vascular resistance in hypertension.

Resistance arteries show accentuated responsiveness to vasoconstrictor agonists in hypertension, and this abnormality relies partly on enhanced Ca^{2+} signaling in vascular smooth muscle (VSM). Although inositol 1,4,5-triphosphate receptors (IP_3Rs) are abundant in VSM, their role in the molecular remodeling of the Ca^{2+} signaling machinery during hypertension has not been addressed. Therefore, we compared IP_3R expression and function between mesenteric arteries of normotensive and hypertensive animals. Levels of IP_3R transcript and protein were significantly increased in mesenteric arteries of hypertensive animals, and pharmacological inhibition of the IP_3R revealed a higher contribution of IP_3-dependent Ca^{2+} release to vascular contraction in these arteries. Subsequently, we established cultured aortic VSM A7r5 cells as a cellular model that replicates IP_3R up-regulation during hypertension by depolarizing the VSM cell membrane. IP_3R up-regulation requires Ca^{2+} influx through L-type Ca^{2+} channels, followed by activation of the calcineurin-NFAT axis, resulting in IP_3R transcription. Functionally, IP_3R up-regulation in VSM is associated with enhancement and sensitization of IP_3-dependent Ca^{2+} release, resulting in increased VSM contraction in response to agonist stimulation.

Hypertension is a complex disease that is the clinical manifestation of multiple genetic, environmental, nutritional, and hormonal pathologies that predispose individuals to cardiovascular disease, including heart failure and stroke (1, 2). In recent years, it has become clear that structural alterations in arteries, referred to as remodeling, increase their stiffness and contribute to the development of hypertension (3, 4). Furthermore, arterial wall injury leads to a phenotypic switch of VSM[2] from a contractile to a proliferative phenotype, which is associated with alterations to the VSM Ca^{2+} signaling machinery (5).

The major drop in hydrostatic pressure in the vasculature occurs at the level of resistance arteries. Because blood flow is proportional to the vessel radius to the 4th power, as described by Poiseuille's law, small changes in the luminal diameter of resistance arteries will dramatically alter resistance to blood flow with a pronounced impact on blood pressure. Peripheral resistance depends on the diameter of resistance arteries, which hinges in part on the contractile state of the VSM cells (6, 7). The resting myogenic tone is set by the summed responses of the Ca^{2+} handling and contractile machineries to various inputs, including sympathetic neurotransmitters (norepinephrine) (8), endothelium-derived agents (NO, endothelin) (6), endocrine factors in the blood stream (angiotensin II) (2), and intraluminal pressure (9).

Several channels and transporters contribute to Ca^{2+} signaling and contraction in VSM, with two primary pathways being the agonist-activated PLC-IP_3R pathway and the voltage-gated L-type Ca^{2+} channel (LTCC) (7). The pore-forming subunit of the LTCC channel in VSM is α_{1C} (10). The fundamental role of these two Ca^{2+} signaling pathways in fueling vasoconstriction during hypertension is attested to clinically by the effective lowering of blood pressure following pharmacological block of the LTCC and α-adrenergic receptors (2). Consistently, norepinephrine produces greater vasoconstriction in hypertensive compared with normotensive individuals (11). However, the molecular mechanisms of this enhanced vasomotor response are unclear.

* This work was supported by a grant from the Qatar National Research Fund, National Priority Research Program Grant NPRP 08-392-3-087. The laboratory of K. M. is also supported by the Biomedical Research Program at Weill Cornell Medical College in Qatar, a program funded by Qatar Foundation.
[S] This article contains supplemental Figs. 1 and 2.
[1] To whom correspondence should be addressed. Tel.: 974-4492-8423; Fax: 974-4492-8422; E-mail: khm2002@qatar-med.cornell.edu.
[2] The abbreviations used are: VSM, vascular smooth muscle; IP_3, inositol 1,4,5-trisphosphate; IP_3R, IP_3 receptor; NFAT, nuclear factor of activated T cells; AHT, angiotensin II-induced hypertension; SAL, saline; $ciIP_3$, caged IP_3; $ciIP_3$, D-2,3-*O*-isopropylidene-6-*O*-(2-nitro-4,5-dimethoxy) benzyl-*myo*-inositol 1,4,5-triphosphate-hexakis(propionoxylmethyl) ester; K20, K40, and K60, 20, 40, and 60 mM KCl, respectively; PLC, phospholipase C; LTCC, L-type Ca^{2+} channel; SHR, spontaneously hypertensive rat(s); Ang II, angiotensin II; SBP, systolic blood pressure; MA, mesenteric arteries; PSS, physiological salt solution; PE, phenylephrine; HBS, HEPES-buffered saline; 2-APB, 2-aminoethoxydiphenyl borate; vWF, von Willebrand factor; SOCE, store-operated Ca^{2+} entry; PMCA, plasma membrane Ca^{2+} pump; Nif, nifedipine; Thaps, thapsigargin; CHX, cycloheximide; ACD, actinomycin D; CsA, cyclosporine A.

The role of the LTCC in modulating the myogenic response of VSM is well established through clinical, genetic, and physiological studies (7, 10, 12–15). In contrast, the contribution of the IP_3R remains poorly characterized. However, several lines of evidence support a role for the PLC-IP_3 axis in regulating the myogenic tone. The IP_3R has been implicated in Ca^{2+}-dependent contraction in response to vasoconstrictors central to blood pressure regulation, including norepinephrine and angiotensin II (16–18). In addition, G-protein-coupled receptor-dependent Ca^{2+} oscillations have been implicated in vasoconstriction (19), and activation of α_1-adrenergic receptors increases the percentage of VSM exhibiting Ca^{2+} oscillations (20). Furthermore, PLC-IP_3-dependent Ca^{2+} release plays an important role in regulating myogenic tone caused by increased intraluminal pressure in isolated arteries (21, 22), and stretch of isolated VSM cells results in enhanced IP_3 levels, leading to Ca^{2+} release (23, 24). Finally, PLC inhibition or Ca^{2+} store depletion results in vasodilation or a decreased myogenic response (25–27). Collectively, these findings suggest that the activity of *in situ* IP_3R is influenced by blood pressure and vasoactive agonists impinging on the VSM cells of resistance arteries.

Here, we report up-regulation of the IP_3R in resistance-size mesenteric arteries in hypertensive mouse and rat models. IP_3R up-regulation could be recapitulated in cultured VSM cells by depolarization-induced activation of the LTCC, leading to induction of the Ca^{2+}-dependent calcineurin-NFAT signaling pathway. Importantly, IP_3R up-regulation results in sensitization of both IP_3-dependent Ca^{2+} release and VSM contraction. Hence, up-regulation of vascular IP_3R is poised to contribute to enhanced Ca^{2+} signaling and vasoreactivity during hypertension.

EXPERIMENTAL PROCEDURES

Animals

All procedures involving animals were approved by the Institutional Animal Care and Use Committee at the University of Arkansas for Medical Sciences. C57BL/6 mice were obtained at 10 weeks of age from Harlan Laboratories (Indianapolis, IN) and maintained in a temperature-controlled room in a 12-h/12-h light/dark cycle with free access to food and water. Wistar Kyoto rats and spontaneously hypertensive rats (SHR) were obtained at 12–14 weeks of age from Taconic Farms (Germantown, NY). Sprague-Dawley rats were obtained from Harlan Laboratories (Madison, WI) at the same age.

Minipump Implantation and Blood Pressure Measurements

Mice were anesthetized by 2.5% isoflurane inhalation. Osmotic minipumps (Alzet 1002, Durect Corp.) loaded with angiotensin II (Ang II; Bachem) to accomplish an infusion dose of 2 ng/min/g for 2 weeks or an equal volume of vehicle (0.9% saline) were implanted subcutaneously. After recovery from anesthesia, mice were housed in individual cages and allowed free access to food and water (28). The systolic blood pressure (SBP) was recorded by tail cuff plethysmography (Kent Scientific) before (day 0) and on days 7 and 14 after osmotic minipump implantation. As described earlier (12, 13), blood pressure was recorded by intra-arterial catheter in anesthetized normotensive and hypertensive rats directly prior to studies.

Vascular Reactivity Assays

Second order mesenteric arteries (MA) were isolated from saline (SAL) and Ang II-infused hypertensive (AHT) mice. Arteries were cleaned of adhered fat and connective tissue in ice-cold physiological salt solution (PSS) of the following composition: 119 mM NaCl, 4.7 mM KCl, 1.17 mM $MgSO_4$, 24 mM $NaHCO_3$, 0.026 mM EDTA, 1.17 mM NaH_2PO_4, 5.5 mM glucose, and 1.6 mM $CaCl_2$. Vessels were cannulated on both ends with tapered glass micropipettes in a microvessel perfusion system (Living Systems) containing PSS bubbled with a 95% O_2, 5% CO_2 gas mixture and maintained at 37 °C. Arteries were perfused with PSS at an intraluminal pressure of 60 mm Hg with no outflow. The PSS in the chamber was exchanged every 15 min during 1 h of equilibration. After equilibration, the viability of MA was verified by observing a contractile response to 60 mM KCl (28). Phenylephrine (PE) concentration-response curves (10^{-8} to 10^{-4} M; half-log increments) were obtained in the absence or presence of the IP_3R blocker, 2-aminoethoxydiphenyl borate (2-APB) (50 μM). Changes in outer vessel diameter were recorded using an upright microscope/Spot RT camera and analyzed with automated edge detection and data acquisition software, DMTvas (Danish Myo Technology). The constrictor response to PE was calculated as percentage change in diameter from the initial resting diameter.

Cell Culture and Transfection

Embryonic rat aortic smooth muscle-derived A7r5 cells were purchased from the American Type Culture Collection (Manassas, VA). The cells were seeded onto a 100-mm dish (BD Biosciences) and grown in Dulbecco's modified Eagle's medium-high glucose supplemented with 4 mM glutamine, 100 units/ml penicillin, 100 μg/ml streptomycin, 1 mM sodium pyruvate, and 10% fetal bovine serum (Sigma). Cells were kept at 37 °C in a humidified atmosphere with 5% CO_2, and fresh medium was added every 48 h until the start of studies.

The plasmid pEGFPC1-NFATc1 was a generous gift from G. Crabtree (Stanford University). A7r5 cells were transiently transfected with pEGFP-NFATc1 using Lipofectamine 2000 (Invitrogen) according to the manufacturer's instructions. At 3 days post-transfection, cells were washed with prewarmed Ca^{2+}/Mg^{2+}-free PBS and maintained for 30 min at 37 °C and 5% CO_2 in HEPES-buffered saline (HBS): 145 mM NaCl, 4 mM KCl, 1 mM $MgCl_2$, 10 mM Hepes, 2 mM $CaCl_2$, 10 mM glucose, pH 7.4. Fluorescent confocal imaging was performed on a Zeiss LSM 710 confocal microscope (Carl Zeiss) using an EC Plan Neofluar ×40/1.3 numerical aperture oil differential interference contrast objective. GFP signal was excited with a 488-nm laser, and emissions were collected through a bandwidth of 492–558 nm. Images were analyzed using ZEN 2008 software (Carl Zeiss).

Western Blotting

Mesenteric Arteries—MA from SAL and AHT mice were carefully isolated and cleaned of adherent fat and connective tissue. Arteries from each mouse were homogenized on ice in radioimmune precipitation assay buffer (Thermo Scientific) containing protease inhibitor mixture (Roche Applied Science). Large tissue debris and cell fragments were removed by centrifu-

gation at 12,000 × *g* at 4 °C for 10 min, and the protein-rich supernatant was carefully collected. Crude protein concentration was determined by the Bradford method using Bio-Rad protein assay dye reagent. Twenty-five μg of protein was loaded per well, and proteins were separated by electrophoresis on a 3–8% polyacrylamide gel (Invitrogen) under reducing conditions. After separation, the proteins were transferred to a PVDF membrane (Thermo Scientific). Membranes were first blocked with 10% nonfat dried milk in TBS-T (10 mM Tris, 100 mM NaCl, and 0.1% Tween 20, pH 7.5) for 1 h at room temperature, followed by overnight incubation at 4 °C with antibodies targeting specific epitopes in 5% nonfat dried milk in TBS-T. In a subset of studies, proteins were similarly prepared from rat MA (12, 13). In Western blots, monoclonal antibodies were directed against IP_3R1 (1:1000; NeuroMab), STIM1 (1:1000; Abcam), PMCA1 (1:500; Santa Cruz Biotechnology, Inc.), and GAPDH (1:10,000; EMD Millipore). Polyclonal antibodies were directed against α_{1C} and TRPC1 (1:1000; Alomone Labs), TRPC4 (1:2000; NeuroMab), or Orai1 (1:1000; ProSci Inc.). After exposure to primary antibody, membranes were incubated for 1 h at room temperature with horseradish peroxidase-labeled sheep anti-mouse IgG or donkey anti-rabbit IgG (GE Healthcare) in TBS-T containing 5% nonfat dried milk. The bands were identified by chemiluminescence and exposed to x-ray films. The density of immunoreactive bands was determined using ImageJ software (National Institutes of Health) and normalized to the GAPDH density for each lane (28). Similar procedures were used to detect rat arterial proteins on Western blot (12, 13).

A7r5 Cells—Total proteins were extracted from A7r5 cells (90–100% confluent) and subjected to Western blot analysis as described above. Forty μg of protein was loaded per well, and expression of Ca^{2+}-handling proteins was detected using specific antibodies against IP_3R1 (1:1000; Millipore), α_{1C} (1:1000; Millipore), TRPC1 (1:200; Santa Cruz Biotechnology), TRPC4 (1:200; Novus Biologicals), STIM1 (1:1000; Cell Signaling Technology), Orai1 (1:1000; Sigma), and PMCA1 (1:500; Santa Cruz Biotechnology). The density of bands was determined using ImageJ and normalized to the α-smooth muscle actin density for each lane.

RT-PCR

Mesenteric Arteries—Total RNA was isolated from MA of SAL and AHT mice using the RNeasy minikit (Qiagen). First strand cDNA synthesis was performed with the iScript™ cDNA synthesis kit (Bio-Rad). After reverse transcription, real-time PCR was performed using iQ™ SYBR® Green Supermix (Bio-Rad) containing a hot start iTaq™ DNA polymerase and the following specific primers: IP_3R1, 5′-GAGATGAGCCTGGCTGAGGTTCAA-3′ (forward) and 5′-TGTTGCCTCCTTCCAGAAGTGCGA-3′ (reverse); β-actin, 5′-ATCCTGTGGCATTCCATGAAACTAC-3′ (forward) and 5′-AGGAGCCAGGGCAGTAATCCTC-3′ (reverse).

Ten pmol of each primer pair and 1 μl of cDNA template were added to the 25-μl reaction mixture, and PCR was performed in an iCycler iQ™ real-time PCR detection system (Bio-Rad) using the following conditions: 5 min at 94 °C for initial activation and 40 cycles of 30 s at 94 °C, 1 min at 65 °C, 2 min at 72 °C, and 10 min at 72 °C. A negative control with RNA instead of cDNA was carried out, and the integrity of PCR was verified by dissociation curve analysis. The relative gene expression was quantified from fluorescence cycle threshold (*Ct*) values using the ΔΔ*Ct* method.

For multicell PCR using populations of enzymatically isolated mouse mesenteric VSM cells, MA were enzymatically digested, and 60–80 VSM cells were aspirated into borosilicate glass micropipette filled with 1× phosphate-buffered saline under the microscope. Total RNA preparation and cDNA synthesis was performed using the Single Cell real-time RT-PCR assay kit (Signosis) per commercial instructions. cDNA products were amplified by nested PCR using gene-specific primer pairs. The following primer pairs were used for first round PCR amplification: IP_3R1, 5′-CCCATCCTAACGGAACGAGC-3′ (forward) and 5′-GGCTTAGCAGCTTTCCAGAAC-3′ (reverse); α_{1C}, 5′-TTACAACCAGCCTCACTGGC-3′ (forward) and 5′-GCGGGAAGTTATCGAACGTG-3′ (reverse); TRPC4, 5′-ACTGCCAATTCTCACCTGGG-3′ (forward) and 5′-GGGCGGAACCATTGCTTAGG-3′ (reverse); α-actin, 5′-TCTGCCCTCTAGCACACAACTG-3′ (forward) and 5′-CTAGCTGTGAAGTCAGTGTCG-3′ (reverse); von Willebrand factor (vWF), 5′-GCTGTGGGAGATGCTTGCCT-3′ (forward) and 5′-TGGAGTACACAGCTTTGCTG-3′ (reverse).

The following gene-specific primers designed within a region of first round PCR products were used for second-round (nested) PCR amplification: IP_3R1, 5′-CTGCTAACCCCTCTCCTGGT-3′ (forward) and 5′-TGGCTGTACAACACAACGGT-3′ (reverse); α_{1C}, 5′-TGTCCCTCTTCAACCGCTTTGACT-3′ (forward) and 5′-GTTCAGCAAGGATGCCACAAGGTT-3′ (reverse); TRPC4, 5′-GGGCGGCGTGCTGCTGAT-3′ (forward) and 5′-CCGCGTTGGCTGACTGTATTGTAG-3′ (reverse); α-actin, 5′-TCTGCCTCTAGCACACAACTG-3′ (forward) and 5′-CTAGGCCAGGGCTACAAGTT-3′ (reverse); vWF, 5′-TTTGTGCAGGGTCAACGAGA-3′ (forward) and 5′-GTACTGCACCTTGGCTGTGA-3′ (reverse).

Reaction conditions for first round PCR and nested PCR were similar to those described above. PCR products were separated by electrophoresis on a 1.6% agarose gel, followed by ethidium bromide staining, UV transillumination, and documentation on Gel/Chemi Doc (Bio-Rad).

A7r5 Cells—Total RNA was prepared from A7r5 cells using TRIzol reagent (Invitrogen). cDNA was synthesized from total RNA using the SuperScript® III first strand synthesis kit (Invitrogen) with random hexamers as primers, according to the manufacturer's instructions. PCRs contained 1 μg of total RNA, 0.2 mM dNTP, Phusion GC Buffer (5×), and Phusion DNA Polymerase (New England Biolabs), and a 0.4 mM concentration of each primer in a total volume of 20 μl. Reactions were run at 94 °C for 2 min, followed by 25 cycles at 94 °C for 30 s, 56 °C for 30 s, and 72 °C for 90 s and a 10-min final extension using the following primers: IP_3R1, 5′-CTCTGTTTGCTGCAAGGGTGATC-3′ (forward) and 5′-GTCCTTCACTTTCACCAGCACG-3′ (reverse); IP_3R2, 5′-ATTGTCACCGTGCTGAACCAG-3′ (forward) and 5′-GCCACAGATGAAGCAGGTTGTC-3′ (reverse); IP_3R3, 5′-CCTGAGATCCTAGAAGAGGACGAG-3′ (forward) and 5′-TCTCCAGACCACAGATGAAGCAC-3′ (reverse); α_{1C}, 5′-CTTCAAACGTGGCCACAGAC-3′ (forward) and 5′-GCTGTGTGGAACTGACGGTA-3′

(reverse); β-actin, 5′-ATCCTGTGGCATTCCATGAAACTAC-3′ (forward) and 5′-AGGAGCCAGGGCAGTAATCTCCT-3′ (reverse).

The amplified products were separated by electrophoresis on 1.2% agarose gels and analyzed as described above. For real-time PCR, each PCR (25 μl) contained 12.5 μl of iQ SYBR Green Supermix (Bio-Rad), 400 nM primers, and an equal volume of cDNA template. Reactions were performed in triplicate on a 7500 Fast Real-Time PCR System (Applied Biosystems) at 95 °C for 10 min and 40 cycles of 20 s at 95 °C, 20 s at 65 °C, and 45 s at 72 °C.

Ca^{2+} Imaging

Cells were seeded onto 35-mm poly-D-lysine-coated glass coverslips (MatTek Corp.) and incubated at 37 °C and 5% CO_2 in complete culture media for 4 days. Cells were incubated with the ratiometric Ca^{2+} dye Fura-2-AM (2 μM; Invitrogen) and placed in the incubator for 45 min in the dark. After incubation, cells were washed with prewarmed Ca^{2+}/Mg^{2+}-free PBS and allowed to rest in HBS for 10 min. The coverslips were then transferred to an inverted epifluorescence microscope (Olympus) equipped with a UPlanSapo ×40/0.95 numerical aperture oil objective and connected to a CCD camera (CoolSNAP HQ^2). The fluorescence emission of individual cells was measured at 510 nm following excitation at 340 and 380 nm using an EasyRatioPro calcium imaging system (PTI). The fluorescence ratio (F_{340}/F_{380}) was recorded in real time at 0.5-s intervals as a relative indicator of intracellular Ca^{2+} concentration. The ratios were calibrated by determining F_{max} and F_{min} values in the presence of 0.1% saponin (F_{max}) and 10 mM EGTA (F_{min}).

Caged IP_3

Ca^{2+} transients were analyzed in A7r5 cells loaded with the membrane-permeant caged IP_3 analog ciIP_3, purchased from SiChem. Briefly, cells were cultured on glass coverslips and kept in culture as described under "Ca^{2+} Imaging." Prior to Ca^{2+} imaging, cells were washed with prewarmed Ca^{2+}/Mg^{2+}-free PBS and incubated in HBS containing 2 μM ciIP_3 for 45 min in the dark, followed by incubation with a 2 μM concentration of the cell-permeant dye Ca-Green-1, AM (Invitrogen), which was added to the loading solution for a further 45 min before washing and allowing at least 30 min for de-esterification. Imaging of changes in $[Ca^{2+}]_i$ was accomplished using an inverted epifluorescence microscope (Olympus) equipped with a UPlanSapo ×40/0.95 numerical aperture oil objective and connected to a CCD camera (CoolSNAP HQ^2). IP_3 was released by a photochemical destruction of the cage with brief exposures (100 ms every 1.5 s) of the cells to UV light (340 nm). The fluorescence of individual cells was collected simultaneously at 510 nm by excitation of Ca-Green-1 at 488 nm using an EasyRatioPro calcium imaging system (PTI). The fluorescence signals are expressed as ratios (F/F_0) of the mean fluorescence F of each cell relative to the mean resting fluorescence F_0.

Monitoring of A7r5 Contraction

Assessment of cell contraction was performed on A7r5 cells cultured on glass coverslips as described above. Attached cells were washed with prewarmed Ca^{2+}/Mg^{2+}-free PBS and allowed to settle in HBS for 10 min prior to live cell imaging. Cell contraction was visualized using an inverted microscope (Olympus) equipped with a LucPlan FLN ×40/0.60 numerical aperture objective. Images were acquired with a CCD camera (Olympus DP72) and processed using DP2-BSW software (Olympus Soft Imaging Solutions). Cell contraction was quantified by morphometric analysis using ImageJ. Briefly, the addition of PE induces the formation of contractile fibers, which appear as protruded edges on the surface of contracted cells. To quantify contractile responses to PE, contractile fibers were quantified using the edge detection function in ImageJ on thresholded time lapse images.

Statistics

Data represent means ± S.E. of the mean for the number (n) of animals or *in vitro* preparations indicated in parentheses. Student's t test was used to compare two data sets, and one-way/two-way analysis of variance and Bonferroni's post hoc test were used for multiple group comparisons. $p \leq 0.05$ was considered significant.

RESULTS AND DISCUSSION

Hypertension Is Coupled to Increased Expression of Vascular IP_3R—To determine the expression level of vascular IP_3R during hypertension, male C57BL/6 mice were infused subcutaneously with Ang II (2 ng/g/min, AHT) for 2 weeks, resulting in average SBP values of 109 ± 2, 136 ± 3, and 152 ± 2 mm Hg at 0, 7, and 14 days, respectively ($n = 12$ each; Fig. 1*A*). In contrast, SBP values were unchanged from the preinfusion value of 105 ± 3 mm Hg in SAL-infused mice ($n = 12$ each; Fig. 1*A*). At 14 days, hypertension correlates with increased protein expression (2.39 ± 0.19-fold) of the type 1 IP_3R (IP_3R1) in MA (Fig. 1, *B* and *C*). Localization and functional studies in renal and mesenteric VSM and in A7r5 cells argue that IP_3R1 is the primary isoform (29–31). Consistently, quantitative RT-PCR reveals a 1.83 ± 0.11-fold increase of IP_3R1 transcript in arteries of AHT compared with SAL mice (Fig. 1*D*).

PE-induced Contractions Are Enhanced in MA of AHT Mice—To assess the functional significance of IP_3R up-regulation in arteries exposed to hypertension, we sought to determine the contribution of IP_3-dependent Ca^{2+} release to vascular contractile responses to the vasoconstrictor agonist, PE. Isolated, pressurized (60 mm Hg) second order MA branches of AHT mice overexpressing IP_3R1 showed accentuated contractions to PE, an α_1-adrenoreceptor agonist that relies on IP_3-dependent Ca^{2+} release for contraction (Fig. 1*E*) (32). The PE-induced contractions in MA from AHT mice averaged 38% higher at agonist concentrations of $\geq 10^{-6}$ M (Fig. 1*F*). The concentration of PE required for half-maximal contraction (ED_{50}) did not differ significantly between MA of SAL (6.9×10^{-7} M) and AHT mice (6.7×10^{-7} M). Subsequently, we observed that the nonselective IP_3R antagonist, 2-APB (33), suppressed contractions to PE in MA of SAL and AHT mice (Fig. 1*E*). Comparison of the amplitude of 2-APB-sensitive contraction between MA of SAL and AHT mice revealed a higher component in arteries from hypertensive animals (Fig. 1, *F* and *G*). These results argue that IP_3-dependent Ca^{2+} release contributes

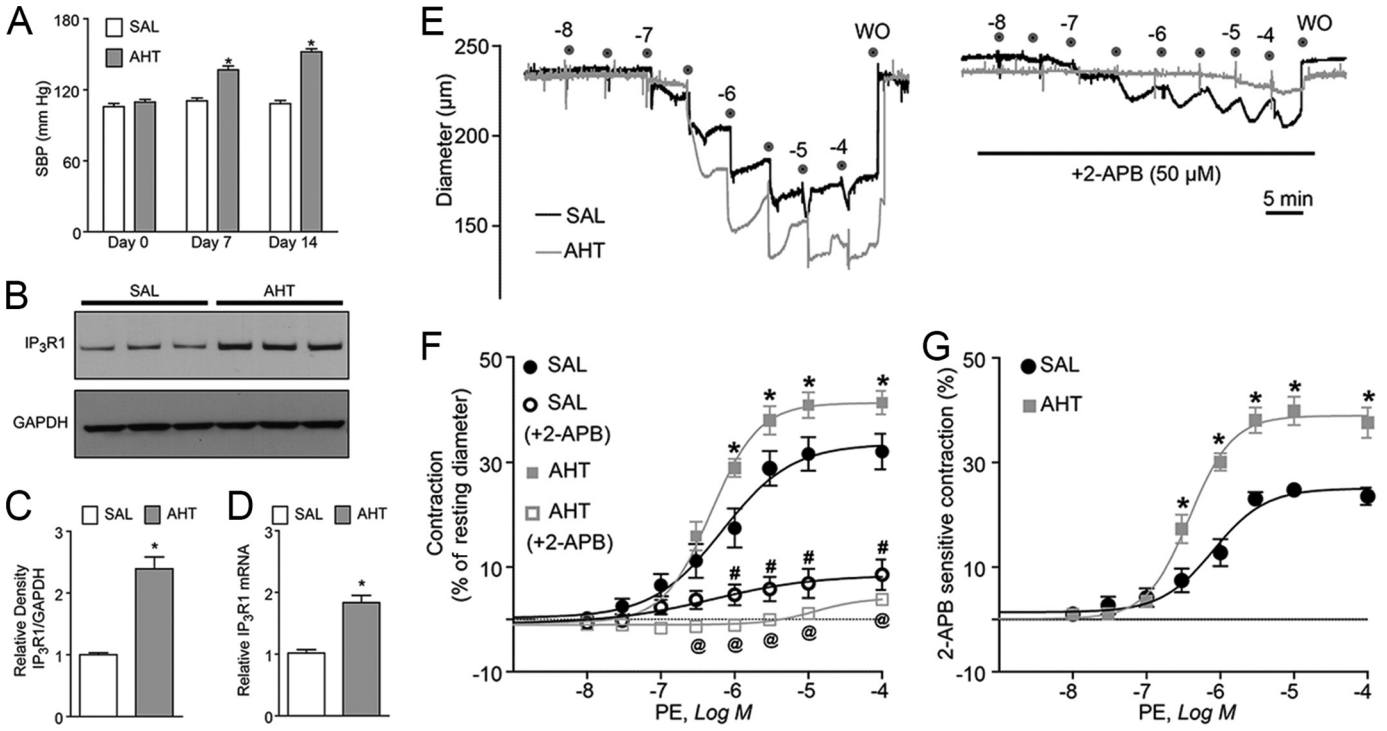

FIGURE 1. **Increased expression and functional contribution of vascular IP$_3$Rs in experimental hypertension.** *A*, measurement of SBP at base line and after infusion of SAL or Ang II to establish AHT. SBP was recorded by tail cuff plethysmography at base line (day 0) and at 7 and 14 days after infusion. SBP was significantly increased in AHT compared with SAL mice at 7 and 14 days ($n = 12$). *B*, immunoblot analysis of IP$_3$R in lysates from mouse MA. Artery lysate from SAL (control) and AHT mice was added to each lane (3 animals/group). *C*, relative protein density after normalization to GAPDH shows that IP$_3$R1 immunoreactivity was 2.4-fold higher in MA of AHT compared with SAL mice ($n = 6$). *D*, quantitative mRNA expression reveals a 1.8-fold increase of IP$_3$R1 transcript in arteries of AHT compared with SAL mice ($n = 4–6$). *Ct* values were normalized to the *Ct* value of the amplification standard β-actin, which was similarly expressed between MA of SAL and AHT mice. *E*, representative traces showing changes in vessel diameter in response to increasing concentrations of PE (*gray dots*). Isolated second order MA from SAL and AHT mice were cannulated and pressurized to 60 mm Hg, and diameter was recorded on-line by edge detection. After washout (*WO*), PE-induced contractions were repeated in the presence of 2-APB (50 μM) (*right*). *F*, concentration-response curves to PE in MA from SAL and AHT mice in the presence (*+2-APB*) or absence of 2-APB. PE-induced contraction was enhanced in arteries of AHT mice ($n = 8$ and 6). PE-induced contraction was inhibited by 2-APB in MA from both SAL and AHT mice ($n = 8$ and 6). *, significant difference between SAL and AHT; @, significant difference between SAL and SAL+2-APB; #, significant difference between AHT and AHT+2-APB. *G*, arteries from AHT mice showed an increased 2-APB-sensitive component of PE-induced contraction compared with SAL mice ($n = 6$ and 8). The 2-APB-sensitive component was calculated by subtracting concentration-dependent contractions to PE obtained in the presence of 2-APB from those obtained in the absence of the blocker. *Error bars*, S.E. *, $p \leq 0.05$.

more significantly to PE-induced vascular contractions in MA of hypertensive animals, supporting a functional role for the observed IP$_3$R up-regulation in increasing vascular reactivity.

Specific Up-regulation of IP$_3$R and α_{1C} in Arteries of AHT Mice—We explored the possibility that Ang II-induced hypertension causes a nonspecific remodeling of Ca^{2+}-handling proteins in VSM by comparing the expression of a panel of proteins implicated in VSM contraction between MA of SAL and AHT mice. It is well known that the α_{1C} pore-forming subunit of the vascular LTCC up-regulates during hypertension (10, 12, 13). This event may partly account for the increased sensitivity of hypertensive subjects to the antihypertensive effect of clinical calcium channel antagonists; these drugs only mildly lower blood pressure in normotensive subjects (34–37). Indeed, Western blots confirmed that α_{1C} up-regulation is coupled to increased IP$_3$R1 expression in MA of AHT mice (Fig. 2*A*). We also evaluated the expression of two agonist-activated TRPC channels implicated in vascular reactivity, TRPC1 and TRPC4 (34–36, 38). TRPC1 expression was unchanged after Ang II infusion, but a pronounced up-regulation of TRPC4 was detected in MA of AHT mice (Fig. 2*A*). However, we failed to detect TRPC4 transcript in multicell PCRs limited to mouse mesenteric VSM cells. In this experiment, PCRs using cDNA derived from whole MA revealed transcripts coding for IP$_3$R1, α_{1C}, TRPC4, α-actin, and vWF; the latter two proteins are VSM and endothelium-specific markers, respectively (Fig. 2*B*, *top*). However, only IP$_3$R1, α_{1C}, and α-actin transcripts were detected in amplified products from isolated VSM cells (Fig. 2*B*, *bottom*). Thus, we ruled out TRPC4 as a direct contributor to VSM contraction, and our data suggest that this channel may only be expressed in the endothelium of small arteries, as suggested by others (34, 35).

Finally, we observed no difference in expression levels of STIM1 and Orai1 between MA of SAL and AHT mice. This finding is significant, because we presumed that the enhanced block of PE-induced contractions by 2-APB in arteries of AH mice reflected an increased contribution of IP$_3$-dependent Ca^{2+} release to VSM reactivity in hypertension (Fig. 1, *E–G*), but 2-APB also can inhibit store-operated Ca^{2+} entry (SOCE) (33, 39, 40), which relies on the endoplasmic reticulum Ca^{2+} sensor STIM1 and the plasma membrane channel Orai1 (41). The comparable expression of STIM1 and Orai1 between MA of SAL and AHT mice is consistent with a relatively minor role of SOCE in VSM contraction and argues that the observed inhibition with 2-APB primarily relates to block of IP$_3$Rs.

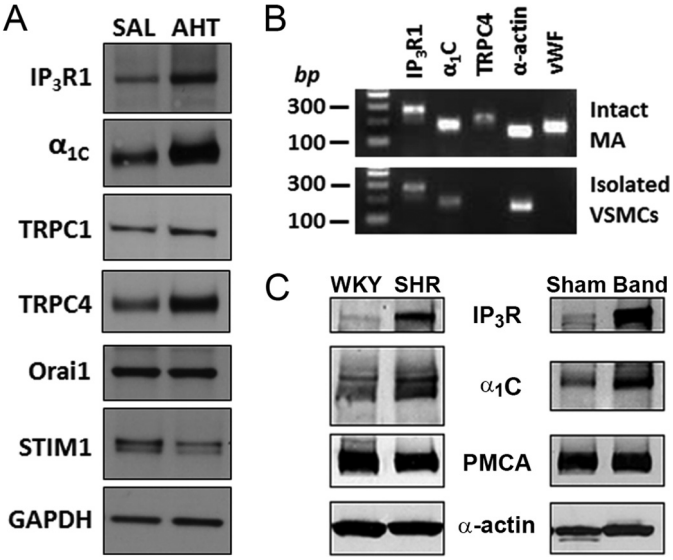

FIGURE 2. **Screening of Ca^{2+}-handling proteins reveals coupled up-regulation of the vascular IP_3R and LTCC in experimental models of hypertension.** *A*, immunoblot analysis of IP_3R1, α_{1C}, TRPC1, TRPC4, Orai1, and STIM1 in lysates from mouse MA. MA lysate pooled from three SAL or AHT mice was added to each lane. Increased expression levels of IP_3R1, α_{1C}, and TRPC4 are detected in MA of AHT mice, whereas levels of TRPC1, Orai1, and STIM1 were similar. *B*, agarose gel analysis of products obtained after PCRs for IP_3R1 (274 bp), α_{1C} (185 bp), and TRPC4 (226 bp) using specific primers. α-Actin (152 bp) and vWF (178 bp) were used as VSM and endothelial cell markers, respectively. IP_3R, α_{1C}, and α-actin were detected both in intact MA and isolated VSM cells as expected. In contrast, TRPC4 and vWF were detected in arteries but not isolated VSM cells, implying expression only in endothelium. *C*, immunoblots comparing the expression of IP_3R, α_{1C}, PMCA, and α-actin (as a loading control) between MA from normotensive Wistar Kyoto rats (*WKY*) and SHR and between MA from sham-operated and aortic-banded (*Band*) hypertensive rats. In each case, lysates were pooled from arteries of three or four rats. Only the IP_3R and α_{1C} proteins are up-regulated in MA from hypertensive SHR and aortic-banded rats. Blots are representative of three experiments.

We also tested if IP_3R up-regulation is specific to the AHT mouse model by evaluating IP_3R1 expression in two rat models of hypertension, the SHR and aortic-banded rat (12, 13). The MA of the genetically hypertensive SHR were compared with those of the normotensive Wistar Kyoto rat. In the second model, the aorta of a Sprague-Dawley rat was partially banded between the left and right renal arteries, thus exposing the entire mesenteric circulation of banded rats to high blood pressure; MA of sham-operated rats exposed to normal blood pressure served as the control. In both rat models of hypertension, the IP_3R1 and the α_{1C} subunit of the LTCC were up-regulated in small MA (Fig. 2*C*). In contrast, expression of a membrane protein involved in Ca^{2+} extrusion, the plasma membrane Ca^{2+} pump (PMCA), was unchanged. Similarly, α-actin used as a loading control showed no change (Fig. 2*C*). We did observe some variability in IP_3R up-regulation in different SHR animals, where in some instances no increase was observed. This may be a reflection of the genetic complexities underlying hypertension in the SHR model. Nonetheless, the fact that IP_3R up-regulation was observed in three distinct models of hypertension with different genetic and neuroendocrine profiles and in two different species argues that it is a general phenomenon associated with hypertension.

Depolarization-induced Ca^{2+} Rise Up-regulates IP_3R in A7r5 Cells—To identify mechanisms that up-regulate IP_3R in VSM and thereby contribute to its overabundance in arteries exposed to hypertension, we used the embryonic rat aortic smooth muscle-derived A7r5 cell line. Notably, pressure-induced depolarization of small arteries and arterioles is recognized as a common abnormality of hypertension, which can induce the up-regulation of LTCCs and trigger enhanced vascular reactivity and vessel remodeling (12, 13). This loss of resting membrane potential (E_m) extends to VSM cells of the renal, mesenteric, and skeletal muscle beds in experimental models of hypertension in which vessels are exposed to high intraluminal pressures (10, 12, 42–45). To mimic a key stimulus of vascular remodeling in hypertension, we exposed aortic A7r5 cells to incrementally higher concentrations of 20 (K20), 40 (K40), and 60 (K60) mM KCl for 24 h, to progressively depolarize and activate the SMCs as an *in vitro* surrogate for the hypertensive environment. These K^+ concentrations would be predicted to shift E_K by +43 mV (K20), +61.5 mV (K40), and +72.4 mV (K60) based on the Nernst potential. All three concentrations of KCl up-regulated the IP_3R protein in A7r5 by 24 h, whereas expression levels of PMCA and smooth muscle α-actin were stable (Fig. 3*A*). Further studies used the lowest depolarizing stimulus of K20 that caused a 1.7-fold increase in IP_3R expression (Fig. 3*E*). Importantly, up-regulation of IP_3R was induced by depolarization rather than the osmotic challenge of K20, because enhanced IP_3R was not observed in A7r5 aortic cells exposed to equiosmolar NaCl or sucrose (*Sucr*) (Fig. 3, *A*, *B*, and *E*). However, up-regulation of IP_3R by 20K was prevented in A7r5 cells incubated in 10 μM nifedipine (Nif), a specific blocker of the LTCC (Fig. 3, *A*, *B*, and *E*). This finding argues that voltage-dependent Ca^{2+} influx through LTCC mediates IP_3R up-regulation.

Similar to arteries exposed to hypertension, depolarization-induced IP_3R up-regulation in A7r5 cells was coupled to an increased expression of LTCC α_{1C} subunit (1.6 ± 0.07-fold; Fig. 3*B*), arguing that depolarization of A7r5 cells faithfully replicates the remodeling of Ca^{2+} signaling pathways observed in arteries from hypertensive animals.

Because SOCE has been previously implicated in VSM proliferation and migration (46), we tested the expression levels of STIM1 and Orai1 following depolarization in A7r5. Consistent with our findings in MA of AHT mice, STIM1 expression levels were stable (Fig. 3*C*), and we were unable to detect Orai1 expression on Western blots from A7r5 cells. Furthermore, no change in the expression levels of TRPC1 was detected in A7r5 cells exposed to KCl (Fig. 3*C*), whereas TRPC4 expression was not detected.

We then tested whether Ca^{2+} influx through LTCC is specifically required for IP_3R up-regulation or whether a nonspecific cytoplasmic Ca^{2+} rise is sufficient to trigger and sustain IP_3R1 enrichment in VSM cells. We raised intracellular Ca^{2+} levels by inhibiting the endoplasmic reticulum Ca^{2+}-ATPase (SERCA) using the specific antagonist thapsigargin (Thaps) (47). Due to a continuous ill defined Ca^{2+} leak pathway at the endoplasmic reticulum membrane, Thaps results in a slow rise in cytoplasmic Ca^{2+} levels. This passive store depletion activates SOCE, thus accentuating the Ca^{2+} rise (43, 48). Indeed, Thaps treatment results in high basal Ca^{2+} levels (Fig. 4*C*) and was sufficient to induce significant IP_3R up-regulation (1.5 + 0.14-fold; Fig. 3, *D* and *E*). Although depolarization-dependent Ca^{2+} influx through LTCC was more efficient at inducing IP_3R up-regulation, the results from Thaps argue that a general cyto-

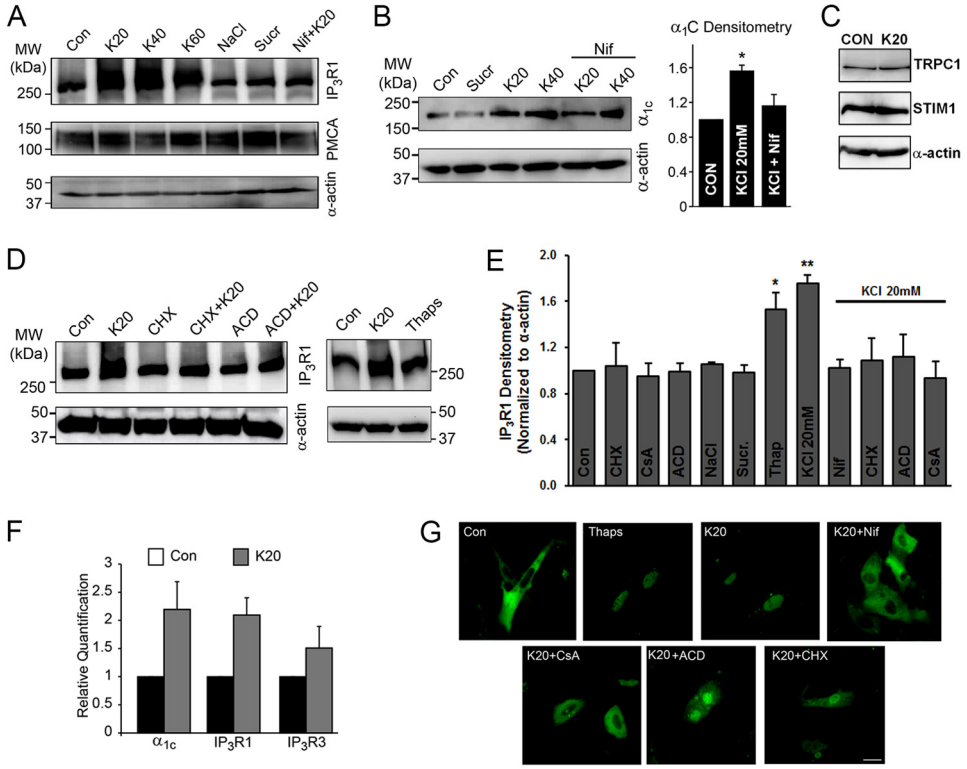

FIGURE 3. **Depolarization of A7r5 cells for 24 h replicates the induction of IP$_3$R and α_{1C} observed in VSM cells of hypertensive animals *in vivo*.** *A–E*, immunoblot analyses of IP$_3$R, PMCA, and α_{1C}. Proteins were isolated from A7r5 cells and separated on SDS-PAGE, and the blots were probed for the appropriate antigens as indicated. *A*, IP$_3$R1 expression is increased in A7r5 cells exposed to K20, K40, or K60 for 24 h but not in cells treated with NaCl or sucrose (*Sucr*) as osmolar controls. Depolarization-induced IP$_3$R up-regulation is lost in the presence of the LTCC blocker, Nif (10 μM). Expression levels of PMCA are unchanged. *B*, the expression level of α_{1C} is significantly increased in A7r5 cells incubated with K20 or K40 for 24 h but not in cells exposed to sucrose or 10 μM Nif ($n = 3$). *C*, expression levels of TRPC1, STIM1, and α-actin are not altered in A7r5 cells depolarized for 24 h by 20K. *D*, *right blot* shows that IP$_3$R1 up-regulates in A7r5 cells exposed to 20K or treated with Thaps (1 μM) for 24 h. The up-regulation of IP$_3$R1 by K20 is blocked by 10 μg/ml CHX or 10 μM ACD. Blots are representative of at least three independent experiments. Smooth muscle-specific α-actin was used as a loading control. *E*, relative immunodensity of the IP$_3$R1 after normalization to α-actin. Cell depolarization with K20 or treatment with Thaps (1 μM) for 24 h increases IP$_3$R1 expression, and this response is lost in the presence Nif (10 μM), CHX (10 μg/ml), ACD (10 μM), or CsA (10 μM) ($n = 3–21$; *, $p < 0.05$; **, $p < 0.01$). *F*, transcriptional up-regulation of IP$_3$R1, IP$_3$R3, and α_{1C} in A7r5 cells depolarized by K20 for 24 h. Real-time PCR plots represent relative quantification. *G*, nuclear translocation of NFATc1 in A7r5 cells. Cells were transfected with plasmids expressing EGFP-NFATc1 and imaged using a confocal laser-scanning microscopy. At rest (*Con*), NFATc1 showed a basal cytoplasmic localization, but treatment with Thaps (1 μM) or K20 alone or in the presence of CHX (10 μg/ml), ACD (10 μM), or CsA (10 μM) promotes its nuclear translocation. In contrast, incubation of cells with 10 μM Nif or CsA prevents K20-induced nuclear translocation of NFATc1. Data are representative of four independent experiments. *Scale bar*, 20 μm. *Error bars*, S.E.

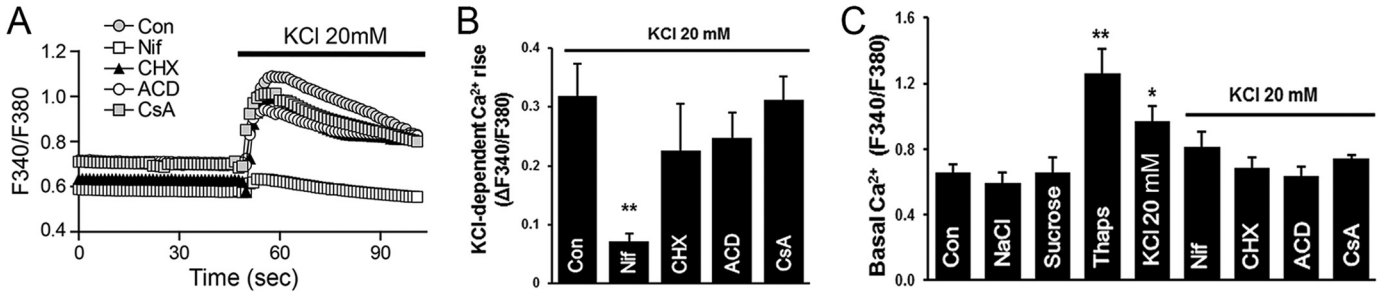

FIGURE 4. **Ca^{2+} dynamics in response to acute KCl depolarization of A7r5 cells.** Cells were loaded with Fura 2-AM and bathed in Ca^{2+}-containing HBS. Imaging was performed as described under "Experimental Procedures." *A*, acute membrane depolarization by K20 results in a global rise in intracellular Ca^{2+}, which is inhibited by Nif (10 μM) but not by ACD (10 μM), CHX (10 μg/liter), or CsA (10 μM). Traces represent average fluorescence intensity of 15–20 individual cells. *B*, quantitation of the K20-induced Ca^{2+} rise as maximal Fura-2 ratio from base line ($\Delta F_{340}/F_{380}$, $n = 4–6$; **, $p < 0.01$). *C*, basal intracellular Ca^{2+} levels were significantly increased in A7r5 cells after 24 h exposure to K20 or 1 μM Thaps. The osmolarity controls NaCl and sucrose did not alter resting Ca^{2+} levels in A7r5 cells. The addition of Nif (10 μM), CHX (10 μg/liter), ACD (10 μM), or CsA (10 μM) before depolarization by K20 prevents the elevation of basal Ca^{2+} level ($n = 3–12$; *, $p < 0.05$; **, $p < 0.01$). *Error bars*, S.E.

plasmic Ca^{2+} rise is sufficient to induce up-regulation of the IP$_3$R in VSM.

Calcium Influx Triggers IP$_3$R Expression through Calcineurin-NFAT Signaling—The establishment of the A7r5 cell model allowed us to identify the signal transduction cascade that mediates depolarization-induced IP$_3$R up-regulation. Studies using quantitative RT-PCR revealed a 2.2 ± 0.4-, 2.1 ± 0.3-, and 1.5 ± 0.3-fold increase of α_{1C}, IP$_3$R1, and the type 3 IP$_3$R (IP$_3$R3) transcripts, respectively, in A7r5 cells exposed to K20 for 24 h (Fig. 3*F*). Similar results were observed in semiquantitative PCR experiments (supplemental Fig. 1), whereas the type 2 IP$_3$R (IP$_3$R2) transcript was not detected.

Block of protein translation with 10 μg/liter cycloheximide (CHX) prevented K20-induced up-regulation of IP_3R at 24 h (Fig. 3, *D* and *E*). Subsequently, nonspecific block of transcription with 10 μM actinomycin D (ACD) also prevented K20-induced IP_3R enrichment (Fig. 3, *C* and *D*). Given that the Ca^{2+}-calmodulin dependent phosphatase, calcineurin, promotes IP_3R abundance in neurons (49), we treated A7r5 cells next with 10 μM cyclosporine A (CsA), a specific calcineurin blocker. CsA also abrogated the increased expression of IP_3R caused by K20 (Fig. 3*E*).

Calcineurin regulates gene expression by dephosphorylating the transcription factor NFAT, which translocates to the nucleus to promote transcription (50). To directly support a role for NFAT in IP_3R up-regulation, we imaged NFATc1 localization in control or K20-depolarized A7r5 cells. Control A7r5 cells transfected with GFP-NFATc1 exhibit a cytosolic distri-

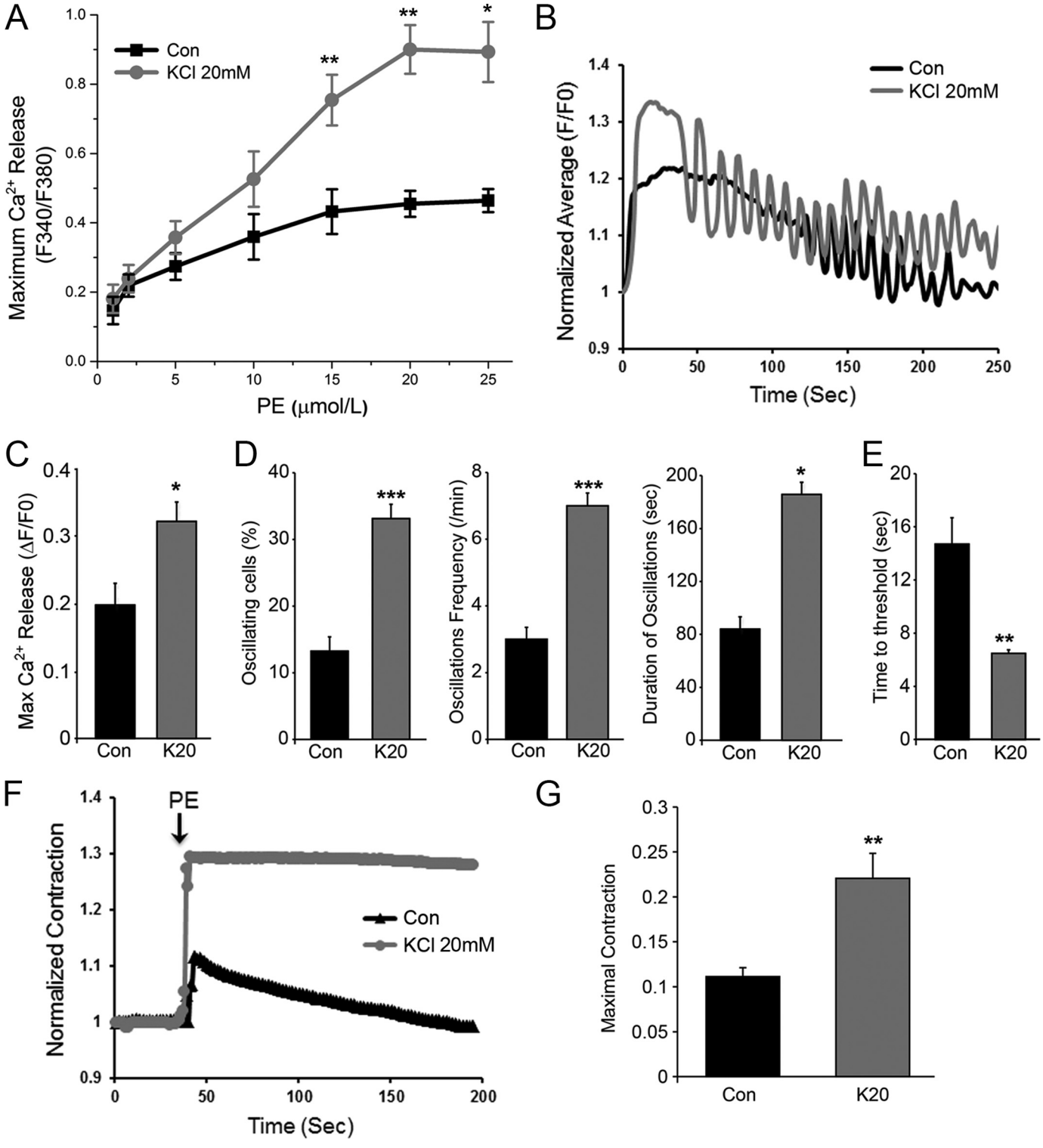

bution (Fig. 3*G*). The addition of K20 induced NFATc1 translocation to the nucleus within 15–20 min. Depolarization-induced NFATc1 translocation was prevented by block of LTCC by Nif or by inhibition of calcineurin activity with CsA (Fig. 3*G*). However, NFATc1 translocation to the nucleus persisted in K20-exposed A7r5 cells pretreated with either CHX or ACD, suggesting that these agents prevent depolarization-induced up-regulation of IP_3R by acting at a site downstream of NFATc1 activation. Notably, we verified that CHX, ACD, and CsA *per se* do not blunt IP_3R up-regulation by directly inhibiting 20K-induced Ca^{2+} influx through LTCCs, whereas Nif blocked the response as expected (Fig. 4, *A* and *B*). Consistent with our earlier finding that exposure of A7r5 cells to Thaps induces IP_3R expression, Thaps treatment also resulted in NFATc1 translocation to the nucleus (Fig. 3*G*). These data support the concept that Ca^{2+} influx through LTCCs activates calcineurin, resulting in translocation of NFATc1 to the nucleus to trigger IP_3R1 transcription.

Given the important role of cytoplasmic Ca^{2+} in mediating IP_3R up-regulation, we were interested in determining the effect of the different treatments on basal Ca^{2+} levels in A7r5 cells. Compared with untreated cells, exposure of A7r5 cells for 24 h to the osmolarity controls (NaCl and sucrose) did not alter basal Ca^{2+} levels (Fig. 4*C*). In contrast, 20K and Thaps significantly increased basal Ca^{2+} levels at 24 h (Fig. 4*C*), findings that correlate well with IP_3R up-regulation under these conditions (Fig. 3*E*). Interestingly, the observed increase in basal Ca^{2+} following 20K treatment was inhibited when cells were pretreated with Nif, CHX, ACD, or CsA (Fig. 4*C*). These results argue that the increased basal Ca^{2+} levels observed after prolonged KCl treatment are not due to Ca^{2+} influx through LTCCs but rather depend critically on IP_3R up-regulation.

IP_3R Up-regulation Sensitizes IP_3-dependent Ca^{2+} Release—To test the consequence of IP_3R up-regulation on IP_3-dependent Ca^{2+} release in response to agonist stimulation, we performed a PE concentration-response curve, which revealed significantly larger Ca^{2+} transients at PE concentration of ≥ 5 μM in K20-treated cells compared with control (*Con*) (Fig. 5*A*). This enhanced Ca^{2+} transient would be predicted to promote VSM contraction. However, the enhanced Ca^{2+} release in response to PE could be due to the remodeling of other components of the signal transduction cascade leading to Ca^{2+} release during the 24-h incubation period and as such may not directly reflect IP_3R function.

To directly assess IP_3R function under conditions where the receptor is up-regulated, we followed the kinetics of IP_3-dependent Ca^{2+} release in A7r5 cells loaded with caged IP_3 ($ciIP_3$) and exposed to UV illumination to rapidly release IP_3, thus mimicking the rapid responses of the receptor/PLC signaling system. Cells were also loaded with the Ca^{2+}-sensitive dye Ca-Green-1 to visualize the ensuing Ca^{2+} dynamics (Fig. 5*B*). We uncaged $ciIP_3$ repeatedly for 100 ms every 1.5 s, which resulted in an initial global sustained Ca^{2+} transient in both control and K20-treated cells (Fig. 5*B*). In a subset of control and K20-treated cells, this was followed by Ca^{2+} oscillations presumably triggered by the oscillatory IP_3 uncaging (Fig. 5*B*). All aspects of IP_3R function exhibited dramatic sensitization in cells with depolarization-induced enriched IP_3R. As expected, maximal Ca^{2+} release measured in both cells that oscillate and those that respond with a monotonic Ca^{2+} rise was significantly increased (Fig. 5*C*). In addition, A7r5 cells exposed to K20 for 24 h to up-regulate IP_3Rs were significantly more likely to oscillate compared with control cells; their oscillation frequency was enhanced dramatically as well as the duration of the oscillations (Fig. 5*D*).

The increased amplitude of Ca^{2+} release in response to IP_3 uncaging is consistent with an increased number of IP_3Rs (Fig. 5*C*). However, the pronounced oscillatory behavior of the K20-treated cells argues that IP_3R sensitivity is also enhanced in cells with up-regulated IP_3R expression. This predicts that K20-treated cells would release Ca^{2+} at lower IP_3 threshold concentrations. To test whether this is the case, we evaluated the time to threshold, which was defined as the time required to produce a Ca^{2+} release signal significantly above the resting base line (empirically determined to $F/F_0 \geq 1.04$). The time to threshold is significantly shorter in K20-treated *versus* control cells, consistent with the conclusion that IP_3R sensitivity is enhanced in A7r5 cells showing overabundant IP_3R.

Therefore, up-regulation of the IP_3R is functionally significant and sensitizes Ca^{2+} release. However, the mechanisms regulating this increased sensitivity require additional investigation. For example, IP_3R up-regulation could be sufficient to mediate the increased sensitivity of IP_3-dependent Ca^{2+} release. Alternatively, the increased mass of the IP_3R could be coupled to post-translational modifications or protein-protein interactions that mediate the enhanced sensitivity of the receptor. Nonetheless, because Ca^{2+} release in our experiments was induced using caged IP_3, the observed enhanced sensitivity of

FIGURE 5. **IP_3R up-regulation sensitizes IP_3-dependent Ca^{2+} release and VSM contraction.** *A*, PE concentration-response curve for Ca^{2+} release in control (*Con*) A7r5 cells or similar cells depolarized by K20 for 24 h to up-regulate IP_3R. Cells were loaded with Fura2-AM and bathed in Ca^{2+}-containing HBS, and images were acquired using an epifluorescence microscope. At low PE concentrations, the two groups of cells had similar fluorescence amplitudes. At PE concentrations above 5 μM, K20-pretreated cells showed higher fluorescence amplitude than control. Values are the mean of fluorescence intensity of 15–20 individual cells for each group given as the relative change in Fura2 fluorescence ratio ($\Delta F_{340}/F_{380}$) ($n = 3$–5, mean ± S.E.; *, $p < 0.05$; **, $p < 0.01$). *B–E*, kinetics of IP_3-dependent Ca^{2+} release evoked by UV photorelease of $ciIP_3$ in A7r5 cells bathed in Ca^{2+}-containing HBS and loaded with $ciIP_3$ and Ca-Green-1. $ciIP_3$ was uncaged by repeated exposure of cells to UV illumination (100 ms every 1.5 s), and the fluorescence of Ca-Green was recorded in real time. *B*, in a subset of cells, $ciIP_3$ uncaging caused an initial global sustained Ca^{2+} transient followed by Ca^{2+} oscillations in both control and 20K-pretreated cells. Cells in both groups also responded to $ciIP_3$ uncaging by a monotonic Ca^{2+} rise without Ca^{2+} oscillations. *C*, the maximal IP_3-dependent Ca^{2+} release was increased in K20-pretreated cells exhibiting enriched IP_3R ($n = 8$; *, $p < 0.05$). *D*, the percentage of oscillating cells ($n = 8$–10; ***, $p < 0.0001$), oscillation frequency/min ($n = 5$–8; ***, $p < 0.0001$), and duration of oscillations ($n = 5$–7; *, $p = 0.05$) were enhanced in K20-pretreated cells. *E*, the time to threshold Ca^{2+} signal was shortened in K20-pretreated cells compared with control ($n = 8$; **, $p < 0.001$). *F*, contractile responses of A7r5 cells to PE (20 μM) in Ca^{2+}-containing HBS were evaluated by imaging of contractile fiber formation. PE results in a transient contractile response in control cells, whereas the contractile response in 20K-pretreated cells is more pronounced and sustained. *G*, statistical analysis of the maximal contractile response to PE of control and K20-pretreated A7r5 cells ($n = 4$; **, $p < 0.05$). *Error bars*, S.E.

IP_3-dependent Ca^{2+} release cannot be due to modulation of the signal transduction cascade upstream of IP_3 production.

Consistent with our findings, an increased IP_3 binding capacity has been reported in the aorta of SHR (51). In addition, in cerebral arteries, the IP_3R was shown to activate Ca^{2+} influx through TRPC3, leading to depolarization and muscle contraction (40). This mechanism, however, is unlikely to contribute to PE-induced Ca^{2+} influx in A7r5 cells that do not express any TRPC3 channels, based on our Western blot analysis (supplemental Fig. 2) and as reported by others (52, 53).

Up-regulation of IP_3R Enhances VSM Contractility—VSM contraction establishes vascular tone and peripheral resistance. Because IP_3R up-regulation is associated with enhanced Ca^{2+} signaling in A7r5 cells, we wondered whether this finding correlates with increased contraction. Thus, we examined the contractile responsiveness of A7r5 cells to PE. A7r5 cells were of the elongated form, and nearly 100% of them contracted upon the addition of PE (20 μM). The extent of contraction was quantified using an imaging approach outlined under "Experimental Procedures," which exploited the appearance of contractile fibers following PE addition. PE results in a transient contractile response in control cells (Fig. 5*F*), whereas A7r5 cells with up-regulated IP_3R (KCl 20 mM) show a significantly more pronounced contractile response that is sustained for the duration of the recording (Fig. 5*F*). Consistently, the mean value of maximal contraction was increased 2 ± 0.02-fold in K20-treated cells when compared with control (Fig. 5*G*).

Collectively, our results show that increased expression of the IP_3R in arterial VSM is consistently associated with hypertension. Depolarization-induced IP_3R up-regulation in A7r5 VSM cells is associated with a higher resting Ca^{2+} level, enhanced response to agonist stimulation, and more robust and sustained contraction. Hence, IP_3R up-regulation observed in VSM cells during hypertension is likely to be an important contributor to enhanced vascular reactivity. As such, the IP_3R represents an attractive potential drug target for the treatment of hypertension.

An increased myogenic response and enhanced reactivity to vasoconstrictor agonists are characteristics of hypertension and contribute significantly to increased blood pressure (54). Multiple factors may act in concert to contribute to the enhanced vascular tone, including an overabundance of Ca^{2+}-conducting channels, such as α_{1C} and TRPC3, alterations in the Ca^{2+} sensitivity of the contractile apparatus in VSM (55), and structural remodeling of arteries (54). With the recognition that the VSM is the mediator of the myogenic response and that a rise in cytoplasmic Ca^{2+} is essential for smooth muscle contraction, it is significant, as shown in this study, that the IP_3R up-regulates in VSM during hypertension, and this event is associated with enhanced IP_3R-mediated Ca^{2+} signaling and VSM contraction. Enrichment of IP_3R can be recapitulated in cultured VSM cells by depolarization-induced opening of LTCC and Ca^{2+}-dependent activation of the calcineurin-NFAT pathway.

Acknowledgments—We are grateful to Aleksandra Pesic, Miodrag Pesic, and Shirley Haun for performing the Western blots in Fig. 2C.

REFERENCES

1. Chockalingam, A. (2008) World Hypertension Day and global awareness. *Can. J. Cardiol.* **24,** 441–444
2. Oparil, S., Zaman, M. A., and Calhoun, D. A. (2003) Pathogenesis of hypertension. *Ann. Intern. Med.* **139,** 761–776
3. Rizzoni, D., and Agabiti-Rosei, E. (2012) Structural abnormalities of small resistance arteries in essential hypertension. *Intern. Emerg. Med.* **7,** 205–212
4. Lemarié, C. A., Tharaux, P. L., and Lehoux, S. (2010) Extracellular matrix alterations in hypertensive vascular remodeling. *J. Mol. Cell Cardiol.* **48,** 433–439
5. House, S. J., Potier, M., Bisaillon, J., Singer, H. A., and Trebak, M. (2008) The non-excitable smooth muscle. Calcium signaling and phenotypic switching during vascular disease. *Pflugers Arch.* **456,** 769–785
6. Bosnjak, Z. J. (1993) Ion channels in vascular smooth muscle. Physiology and pharmacology. *Anesthesiology* **79,** 1392–1401
7. Hill, M. A., Zou, H., Potocnik, S. J., Meininger, G. A., and Davis, M. J. (2001) Arteriolar smooth muscle mechanotransduction. Ca^{2+} signaling pathways underlying myogenic reactivity. *J. Appl. Physiol.* **91,** 973–983
8. Hirst, G. D., and Edwards, F. R. (1989) Sympathetic neuroeffector transmission in arteries and arterioles. *Physiol. Rev.* **69,** 546–604
9. Folkow, B. (1982) Physiological aspects of primary hypertension. *Physiol. Rev.* **62,** 347–504
10. Cox, R. H., and Rusch, N. J. (2002) New expression profiles of voltage-gated ion channels in arteries exposed to high blood pressure. *Microcirculation* **9,** 243–257
11. Ziegler, M. G., Mills, P., and Dimsdale, J. E. (1991) Hypertensives' pressor response to norepinephrine. Analysis by infusion rate and plasma levels. *Am. J. Hypertens.* **4,** 586–591
12. Pesic, A., Madden, J. A., Pesic, M., and Rusch, N. J. (2004) High blood pressure upregulates arterial L-type Ca^{2+} channels. Is membrane depolarization the signal? *Circ. Res.* **94,** e97–e104
13. Pratt, P. F., Bonnet, S., Ludwig, L. M., Bonnet, P., and Rusch, N. J. (2002) Upregulation of L-type Ca^{2+} channels in mesenteric and skeletal arteries of SHR. *Hypertension* **40,** 214–219
14. Nelson, M. T., Patlak, J. B., Worley, J. F., and Standen, N. B. (1990) Calcium channels, potassium channels, and voltage dependence of arterial smooth muscle tone. *Am. J. Physiol.* **259,** C3–C18
15. Moosmang, S., Schulla, V., Welling, A., Feil, R., Feil, S., Wegener, J. W., Hofmann, F., and Klugbauer, N. (2003) Dominant role of smooth muscle L-type calcium channel Cav1.2 for blood pressure regulation. *EMBO J.* **22,** 6027–6034
16. Somlyo, A. V., Bond, M., Somlyo, A. P., and Scarpa, A. (1985) Inositol trisphosphate-induced calcium release and contraction in vascular smooth muscle. *Proc. Natl. Acad. Sci. U.S.A.* **82,** 5231–5235
17. Hashimoto, T., Hirata, M., Itoh, T., Kanmura, Y., and Kuriyama, H. (1986) Inositol 1,4,5-trisphosphate activates pharmacomechanical coupling in smooth muscle of the rabbit mesenteric artery. *J. Physiol.* **370,** 605–618
18. Smith, J. B. (1986) Angiotensin-receptor signaling in cultured vascular smooth muscle cells. *Am. J. Physiol.* **250,** F759–F769
19. Perez, J. F., and Sanderson, M. J. (2005) The contraction of smooth muscle cells of intrapulmonary arterioles is determined by the frequency of Ca^{2+} oscillations induced by 5-HT and KCl. *J. Gen. Phys.* **125,** 555–567
20. Miriel, V. A., Mauban, J. R., Blaustein, M. P., and Wier, W. G. (1999) Local and cellular Ca^{2+} transients in smooth muscle of pressurized rat resistance arteries during myogenic and agonist stimulation. *J. Physiol.* **518,** 815–824
21. Matsumoto, H., Baron, C. B., and Coburn, R. F. (1995) Smooth muscle stretch-activated phospholipase C activity. *Am. J. Physiol.* **268,** C458–C465
22. Narayanan, J., Imig, M., Roman, R. J., and Harder, D. R. (1994) Pressurization of isolated renal arteries increases inositol trisphosphate and diacylglycerol. *Am. J. Physiol.* **266,** H1840–H1845
23. Kulik, T. J., Bialecki, R. A., Colucci, W. S., Rothman, A., Glennon, E. T., and Underwood, R. H. (1991) Stretch increases inositol trisphosphate and inositol tetrakisphosphate in cultured pulmonary vascular smooth muscle cells. *Biochem. Biophys. Res. Commun.* **180,** 982–987

24. Davis, M. J., and Hill, M. A. (1999) Signaling mechanisms underlying the vascular myogenic response. *Physiol. Rev.* **79,** 387–423
25. Inscho, E. W., Cook, A. K., Mui, V., and Imig, J. D. (1998) Calcium mobilization contributes to pressure-mediated afferent arteriolar vasoconstriction. *Hypertension* **31,** 421–428
26. Osol, G., Laher, I., and Kelley, M. (1993) Myogenic tone is coupled to phospholipase C and G protein activation in small cerebral arteries. *Am. J. Physiol.* **265,** H415–H420
27. Watanabe, J., Karibe, A., Horiguchi, S., Keitoku, M., Satoh, S., Takishima, T., and Shirato, K. (1993) Modification of myogenic intrinsic tone and $[Ca^{2+}]_i$ of rat isolated arterioles by ryanodine and cyclopiazonic acid. *Circ. Res.* **73,** 465–472
28. Kharade, S. V., Sonkusare, S. K., Srivastava, A. K., Thakali, K. M., Fletcher, T. W., Rhee, S. W., and Rusch, N. J. (2013) The β3 subunit contributes to vascular calcium channel upregulation and hypertension in angiotensin II-infused C57BL/6 mice. *Hypertension* **61,** 137–142
29. Monkawa, T., Hayashi, M., Miyawaki, A., Sugiyama, T., Yamamoto-Hino, M., Hasegawa, M., Furuichi, T., Mikoshiba, K., and Saruta, T. (1998) Localization of inositol 1,4,5-trisphosphate receptors in the rat kidney. *Kidney Int.* **53,** 296–301
30. Grayson, T. H., Haddock, R. E., Murray, T. P., Wojcikiewicz, R. J., and Hill, C. E. (2004) Inositol 1,4,5-trisphosphate receptor subtypes are differentially distributed between smooth muscle and endothelial layers of rat arteries. *Cell Calcium* **36,** 447–458
31. Wang, Y., Chen, J., Wang, Y., Taylor, C. W., Hirata, Y., Hagiwara, H., Mikoshiba, K., Toyo-oka, T., Omata, M., and Sakaki, Y. (2001) Crucial role of type 1, but not type 3, inositol 1,4,5-trisphosphate (IP_3) receptors in IP_3-induced Ca^{2+} release, capacitative Ca^{2+} entry, and proliferation of A7r5 vascular smooth muscle cells. *Circ. Res.* **88,** 202–209
32. Lee, C. H., Poburko, D., Sahota, P., Sandhu, J., Ruehlmann, D. O., and van Breemen, C. (2001) The mechanism of phenylephrine-mediated $[Ca^{2+}]_i$ oscillations underlying tonic contraction in the rabbit inferior vena cava. *J. Physiol.* **534,** 641–650
33. Maruyama, T., Kanaji, T., Nakade, S., Kanno, T., and Mikoshiba, K. (1997) 2APB, 2-aminoethoxydiphenyl borate, a membrane-penetrable modulator of Ins(1,4,5)P_3-induced Ca^{2+} release. *J. Biochem.* **122,** 498–505
34. Freichel, M., Suh, S. H., Pfeifer, A., Schweig, U., Trost, C., Weissgerber, P., Biel, M., Philipp, S., Freise, D., Droogmans, G., Hofmann, F., Flockerzi, V., and Nilius, B. (2001) Lack of an endothelial store-operated Ca^{2+} current impairs agonist-dependent vasorelaxation in $TRP4^{-/-}$ mice. *Nat. Cell Biol.* **3,** 121–127
35. Bergdahl, A., Gomez, M. F., Dreja, K., Xu, S. Z., Adner, M., Beech, D. J., Broman, J., Hellstrand, P., and Swärd, K. (2003) Cholesterol depletion impairs vascular reactivity to endothelin-1 by reducing store-operated Ca^{2+} entry dependent on TRPC1. *Circ. Res.* **93,** 839–847
36. Xu, S. Z., and Beech, D. J. (2001) TrpC1 is a membrane-spanning subunit of store-operated Ca^{2+} channels in native vascular smooth muscle cells. *Circ. Res.* **88,** 84–87
37. Takata, Y., and Hutchinson, J. S. (1983) Exaggerated hypotensive responses to calcium antagonists in spontaneously hypertensive rats. *Clin. Exp. Hypertens. A* **5,** 827–847
38. Bergdahl, A., Gomez, M. F., Wihlborg, A. K., Erlinge, D., Eyjolfson, A., Xu, S. Z., Beech, D. J., Dreja, K., and Hellstrand, P. (2005) Plasticity of TRPC expression in arterial smooth muscle. Correlation with store-operated Ca^{2+} entry. *Am. J. Physiol. Cell Physiol.* **288,** C872–C880
39. DeHaven, W. I., Smyth, J. T., Boyles, R. R., Bird, G. S., and Putney, J. W., Jr. (2008) Complex actions of 2-aminoethyldiphenyl borate on store-operated calcium entry. *J. Biol. Chem.* **283,** 19265–19273
40. Xi, Q., Adebiyi, A., Zhao, G., Chapman, K. E., Waters, C. M., Hassid, A., and Jaggar, J. H. (2008) IP_3 constricts cerebral arteries via IP_3 receptor-mediated TRPC3 channel activation and independently of sarcoplasmic reticulum Ca^{2+} release. *Circ. Res.* **102,** 1118–1126
41. Cahalan, M. D. (2009) STIMulating store-operated Ca^{2+} entry. *Nat. Cell Biol.* **11,** 669–677
42. Stekiel, W. J., Contney, S. J., and Lombard, J. H. (1986) Small vessel membrane potential, sympathetic input, and electrogenic pump rate in SHR. *Am. J. Physiol.* **250,** C547–C556
43. Stekiel, W. J., Contney, S. J., and Lombard, J. H. (1991) Sympathetic neural control of vascular muscle in reduced renal mass hypertension. *Hypertension* **17,** 1185–1191
44. Rusch, N. J., and Stekiel, W. J. (1991) Ionic channels of vascular smooth muscle in hypertension. in *Cellular and Molecular Mechanisms of Hypertension* (Cox, R. H., ed) pp. 1–7, Plenum Press, New York
45. Stekiel, W. J., Contney, S. J., and Rusch, N. J. (1993) Altered β-receptor control of *in situ* membrane potential in hypertensive rats. *Hypertension* **21,** 1005–1009
46. Potier, M., Gonzalez, J. C., Motiani, R. K., Abdullaev, I. F., Bisaillon, J. M., Singer, H. A., and Trebak, M. (2009) Evidence for STIM1- and Orai1-dependent store-operated calcium influx through ICRAC in vascular smooth muscle cells. Role in proliferation and migration. *FASEB J.* **23,** 2425–2437
47. Thastrup, O., Dawson, A. P., Scharff, O., Foder, B., Cullen, P. J., Drøbak, B. K., Bjerrum, P. J., Christensen, S. B., and Hanley, M. R. (1989) Thapsigargin, a novel molecular probe for studying intracellular calcium release and storage. *Agents Actions* **27,** 17–23
48. Parekh, A. B., and Putney, J. W., Jr. (2005) Store-operated calcium channels. *Physiol. Rev.* **85,** 757–810
49. Genazzani, A. A., Carafoli, E., and Guerini, D. (1999) Calcineurin controls inositol 1,4,5-trisphosphate type 1 receptor expression in neurons. *Proc. Natl. Acad. Sci. U.S.A.* **96,** 5797–5801
50. Rao, A., Luo, C., and Hogan, P. G. (1997) Transcription factors of the NFAT family. Regulation and function. *Annu. Rev. Immunol.* **15,** 707–747
51. Bernier, S., and Guillemette, G. (1993) Increased inositol 1,4,5-trisphosphate binding capacity in vascular smooth muscle of spontaneously hypertensive rats. *Am. J. Hypertens.* **6,** 217–225
52. Jung, S., Strotmann, R., Schultz, G., and Plant, T. D. (2002) TRPC6 is a candidate channel involved in receptor-stimulated cation currents in A7r5 smooth muscle cells. *Am. J. Physiol. Cell Physiol.* **282,** C347–C359
53. Soboloff, J., Spassova, M., Xu, W., He, L. P., Cuesta, N., and Gill, D. L. (2005) Role of endogenous TRPC6 channels in Ca^{2+} signal generation in A7r5 smooth muscle cells. *J. Biol. Chem.* **280,** 39786–39794
54. Baek, E. B., and Kim, S. J. (2011) Mechanisms of myogenic response. Ca^{2+}-dependent and -independent signaling. *J. Smooth Muscle Res.* **47,** 55–65
55. Schubert, R., Lidington, D., and Bolz, S. S. (2008) The emerging role of Ca^{2+} sensitivity regulation in promoting myogenic vasoconstriction. *Cardiovasc. Res.* **77,** 8–18